

**High Hole Mobility and Nonsaturating Giant Magnetoresistance in the New 2D  
Metal NaCu<sub>4</sub>Se<sub>4</sub> Synthesized by a Unique Pathway**

Haijie Chen,<sup>1,2</sup> João N. B. Rodrigues,<sup>3</sup> Alexander J. E. Rettie,<sup>1</sup> Tze-Bin Song,<sup>2</sup> Daniel G.  
Chica,<sup>2</sup> Xianli Su,<sup>2</sup> Jin-Ke Bao,<sup>1</sup> Duck Young Chung,<sup>1</sup> Wai-Kwong Kwok,<sup>1</sup> Lucas K.  
Wagner,<sup>3</sup> and Mercuri G. Kanatzidis\*,<sup>1,2</sup>

<sup>1</sup>*Materials Science Division, Argonne National Laboratory, Argonne, Illinois 60439,  
United States*

<sup>2</sup>*Department of Chemistry, Northwestern University, Evanston, Illinois 60208, United  
States*

<sup>3</sup>*Department of Physics, University of Illinois at Urbana-Champaign, Illinois 61801,  
United States*

**Abstract:** The new compound  $\text{NaCu}_4\text{Se}_4$  forms by the reaction of  $\text{CuO}$  and  $\text{Cu}$  in a molten sodium polyselenide flux, with the existence of  $\text{CuO}$  being unexpectedly critical to its synthesis. It adopts a layered hexagonal structure (space group  $P6_3/mmc$  with cell parameters  $a = 3.9931(6) \text{ \AA}$  and  $c = 25.167(5) \text{ \AA}$ ), consisting of infinite two-dimensional (2D)  $[\text{Cu}_4\text{Se}_4]^-$  slabs separated by  $\text{Na}^+$  cations. X-ray photoelectron spectroscopy suggests that  $\text{NaCu}_4\text{Se}_4$  is mixed-valent with the formula  $(\text{Na}^+)(\text{Cu}^+)_4(\text{Se}^{2-})(\text{Se}^-)(\text{Se}_2)^{2-}$ .  $\text{NaCu}_4\text{Se}_4$  is a  $p$ -type metal with a carrier density of  $\sim 10^{21} \text{ cm}^{-3}$  and a high hole mobility of  $\sim 808 \text{ cm}^2 \text{ V}^{-1} \text{ s}^{-1}$  at 2 K based on electronic transport measurements. First-principles calculations suggest the density of states around the Fermi level are composed of  $\text{Cu-}d$  and  $\text{Se-}p$  orbitals. At 2 K, a very large transverse magnetoresistance of  $\sim 1400\%$  was observed, with a nonsaturating, linear dependence on field up to 9 T. Our results indicate that the use of metal oxide chemical precursors can open reaction paths to new low-dimensional compounds.

**Keywords:** two-dimensional material; metal; magnetoresistance; flux synthesis

## Introduction

The ternary copper chalcogenides  $A/Cu/Q$  ( $A = Na, K, Rb, Cs, Tl$ ;  $Q = S, Se, Te$ ) are a family with rich structural and compositional diversity. These compounds host phase transitions,<sup>1</sup> modulated superlattices,<sup>2-3</sup> massive copper vacancies,<sup>4-5</sup> and are of interest in energy harvesting and conversion, including but not limited to: solid-state supercapacitors,<sup>6-7</sup> and ionic conductors.<sup>8</sup> All structural dimensionalities are found in this class, for example, the one-dimensional (1D)  $Na_3Cu_4S_4$ ,<sup>9-10</sup> the two-dimensional (2D)  $ACu_4Q_3$  ( $A = Na, K, Rb, Cs, Tl$ ;  $Q = S, Se$ ),<sup>11-12</sup>  $NaCu_4S_4$ ,<sup>13</sup>  $A_4Cu_8Te_{10}$  ( $A = Rb, Cs$ ),<sup>14</sup>  $NaCu_6Se_4$ ,<sup>15</sup>  $TlCu_2Se_2$ ,<sup>16</sup> and the three-dimensional (3D)  $K_4Cu_8Te_{11}$ ,<sup>14</sup>  $Cs_3Cu_{20}Te_{13}$ ,<sup>17</sup> to name a few. Generally, they can be classified by the electronic structure and have two different general categories: mixed-valent and valence-precise compounds. The former tend to form metals, whereas the latter are semiconductors. In the mixed-valent systems, only  $Cu^+$  is present in the chalcogenide network rather than  $Cu^{2+}$ , and the mixed valency exists mainly on the chalcogen part and generally in the form of delocalized holes leading to *p*-type transport.

The low-melting flux synthesis method, which gives access to intermediate temperatures, has been proven a powerful approach to discover new phases in the  $A/Cu/Q$  system.<sup>18-19</sup> Despite the great success of the polychalcogenide flux method in enabling productive synthesis routes to new materials, e.g.,  $KCu_{3-x}Se_2$ ,<sup>5</sup>  $NaCu_4Se_3$ ,<sup>12</sup> and  $NaCu_6Se_4$ ,<sup>15</sup> in rare instances we also discover that the nature of the precursors can also be critical in forming new phases. For example, the use of  $Cu_2O$  was shown to be unique in obtaining the mixed-anion oxychalcogenide compound  $Na_{1.9}Cu_2Se_2 \cdot Cu_2O$  which features metallic behavior with mixed valency.<sup>20</sup>

In this work, we report that the use of CuO as starting precursor in sodium polyselenide flux uniquely leads to the new phase NaCu<sub>4</sub>Se<sub>4</sub> with a special 2D structure related to that of CuSe. It is composed of alternating Na<sup>+</sup> cations and [Cu<sub>4</sub>Se<sub>4</sub>]<sup>-</sup> slabs. The use of CuO as a source of Cu atoms was found to be necessary to form the layered NaCu<sub>4</sub>Se<sub>4</sub>, and to avoid the closely related 2D compounds NaCu<sub>4</sub>Se<sub>3</sub><sup>12</sup> and NaCu<sub>6</sub>Se<sub>4</sub><sup>15</sup>, despite the fact that no oxygen incorporates in the final product. Unlike NaCu<sub>4</sub>Se<sub>3</sub><sup>12</sup> and NaCu<sub>6</sub>Se<sub>4</sub><sup>15</sup>, the metallic NaCu<sub>4</sub>Se<sub>4</sub> features a high hole mobility of ~808 cm<sup>2</sup> V<sup>-1</sup> s<sup>-1</sup> at 2 K, with a nonsaturating, large and linear magnetoresistance (MR) of ~1400% at ±9 T. It is noted that the MR in a metal usually varies only by several percent.<sup>21</sup> Therefore, the behavior of NaCu<sub>4</sub>Se<sub>4</sub> is surprising because it is a metallic compound and because the effect of nonsaturating linear MR is typically observed in special semiconductors (e.g. Ag<sub>2</sub>Q (Q = Se, Te)),<sup>22-24</sup> topological insulators (e.g. Na<sub>3</sub>Bi,<sup>25-26</sup> and Cd<sub>3</sub>As<sub>2</sub><sup>27</sup>), Weyl semimetals (e.g. NbP,<sup>28</sup> TaAs<sup>29</sup>), and nodal semimetals (e.g. ZrSiQ (Q = S, Se, Te)).<sup>30-31</sup> To our knowledge, NaCu<sub>4</sub>Se<sub>4</sub> is the first copper chalcogenide reported to exhibit nonsaturating, large and linear MR. Current interest in low dimensional materials exhibiting not only large but nonsaturating magnetoresistance is intense because of implications of special quantum properties that such materials may harbor.<sup>32</sup>

## Experimental Section

**Reagents.** The following chemicals were used as purchased: copper powder (99.9%, Sigma-Aldrich), sodium chunks (99.99%, Sigma-Aldrich), CuO powder (99.9%, Sigma-Aldrich) and selenium shot (99.999%, American Elements). Na<sub>2</sub>Se was synthesized by reacting stoichiometric amounts of the elements in liquid ammonia.<sup>33-34</sup>

**Synthesis.** All chemical handling was carried out in a dry nitrogen-filled glovebox. In a typical synthesis, Na<sub>2</sub>Se (0.375 g, 3 mmol), CuO (0.080 g, 1 mmol), Cu (0.064 g, 1 mmol), and Se (0.632 g, 8 mmol) were thoroughly mixed and placed into a carbon-coated fused-silica tube (12 mm O.D. × 10 mm I.D.). The mixture was then evacuated to <10<sup>-4</sup> mbar and flame-sealed. The ampule was heated to 873 K in 10 h, soaked there for 20 h, and then slowly cooled at a rate of -5 °C/h to room temperature. Excess polyselenide flux in the resulting ingot-like product was removed by washing with *N,N'*-dimethylformamide under flowing N<sub>2</sub>. After finally washing with diethyl ether and drying, thin dark blue hexagonal plate crystals as a major product and light-yellow colored powders, at about 10% portion of the product, were obtained. The powders were found to be Na<sub>2</sub>O<sub>2</sub>. The single crystals were found to consist of NaCu<sub>4</sub>Se<sub>4</sub> (~80% yield) and NaCu<sub>6</sub>Se<sub>4</sub> (~20% yield). The NaCu<sub>4</sub>Se<sub>4</sub> crystals were stable in ambient conditions. EDS yields of the NaCu<sub>4</sub>Se<sub>4</sub> crystals gave Na:Cu:Se atomic ratios of ~1:4:4 (Table S1 in the Supporting Information). PXRD of the reaction product agrees well with the simulated pattern from the single-crystal structure solution, with NaCu<sub>6</sub>Se<sub>4</sub> as a minor phase (Figure S1).

**Single-Crystal X-ray Diffraction.** A well-defined single crystal (600 μm × 500 μm × 100 μm) was mounted on a glass fiber. Diffraction data was collected on a single-crystal diffractometer (STOE IPDS 2T) at room temperature (293 K) and 50 kV and 40 mA with graphite-monochromatized Mo K<sub>α</sub> radiation ( $\lambda = 0.71073 \text{ \AA}$ ).<sup>35</sup> Each data frame was collected with an exposure time of 5 min and  $\omega$  rotation of 1°. No significant degradation of the single crystal was observed during the measurement. The X-RED and X-SHAPE software packages were used for data integration and analytical absorption corrections.<sup>35</sup> The crystal structure was solved by direct methods and refined with the SHELX software

package.<sup>36</sup> Summarized crystal structure and refinement information are given in Tables 1-4.

**X-ray Photoelectron Spectroscopy (XPS).** Single crystals used for XPS was pre-screened on the STOE IPDS 2T to check the structural parameters. XPS was collected to identify the valence states of elements in the compound by using an ESCALab250i-XL electron spectrometer (Thermo Scientific) with 300 W Al  $K_{\alpha}$  radiation. The base pressure was  $\sim 3 \times 10^{-9}$  mbar. The binding energies were referenced to the  $C_{1s}$  line at 284.8 eV from adventitious carbon.

**Electronic Transport Measurements.** Charge transport property measurements were carried out on a  $\text{NaCu}_4\text{Se}_4$  single crystal (dimensions:  $1 \times 0.5 \times 0.1 \text{ mm}^3$ ) which was confirmed on the STOE IPDS 2T. The data were obtained using a Dynacool Physical Property Measurement System (PPMS, Quantum Design) from 2 to 300 K. The resistivity was measured in a four-point collinear geometry and the Hall effect from  $\pm 9$  T was measured by placing two voltage contacts perpendicular to the axis of the current flow. The magnetic field was applied perpendicular to the plate crystal and the plane of current flow. The Hall resistivity ( $\rho_{xy}$ ), was obtained via  $\rho_{xy} = [\rho_{(+H)} - \rho_{(-H)}]/2$ . The magnetoresistance (MR) was defined by  $\Delta\rho/\rho_0 = [\rho(H) - \rho(0)]/\rho(0) \times 100\%$ .<sup>37-38</sup> The angular dependence of the magnetoresistance was collected using the rotator option (Quantum Design). The use of silver paste on  $\text{NaCu}_4\text{Se}_4$  resulted in unstable contact resistances. To form stable, Ohmic contact, Pt pads ( $\sim 50$  nm thick) were sputtered before 25  $\mu\text{m}$  gold wires were attached using Ag paste (DuPont 4929N).<sup>5</sup> Relevant dimensions (length, width, and thickness) were measured from an SEM image of the sample.

**Heat Capacity.** The heat capacity ( $C$ ) of  $\text{NaCu}_4\text{Se}_4$  was measured using a relaxation method in the PPMS. A number of crystals were manually selected and positioned on the sapphire platform using Apiezon N grease. It was measured in a temperature range of 4 – 10 K. The data is analyzed by the formula  $C(T) = \gamma T + \beta_1 T^3 + \beta_2 T^5$  in which  $\gamma T$  and  $\beta_1 T^3 + \beta_2 T^5$  are the electron and phonon contributions, respectively.<sup>39</sup> The Debye temperature,  $\Theta_D$ , is calculated by  $\Theta_D = (12\pi^4 N R / 5\beta)^{1/3}$  in which  $N = 9$  is the number of atoms per formula unit and  $R$  is the gas constant. The effective mass  $m^*$  is estimated by the relationship with  $\gamma = \pi^2 / 3 \kappa_B^2 N(E_F) = 1.36 \times 10^{-4} \times V_{\text{mol}}^{2/3} n_V^{1/3} m^* / m_0$ ,<sup>40</sup> where  $V_{\text{mol}}$ ,  $n_V$ , and  $m^* / m_0$  are molar volume, carrier concentration per atom, and effective mass, respectively.

**First-Principles Calculations.** The electronic structure of  $\text{NaCu}_4\text{Se}_4$  was obtained by performing *ab initio* calculations based on density functional theory. We employed the Kohn-Sham density functional theory (KS-DFT) approach, as implemented in the QUANTUM ESPRESSO code.<sup>41-42</sup> The exchange-correlation energy was approximated by the generalized gradient approximation (GGA) using the Perdew-Burke-Ernzerhof (PBE) functional.<sup>43</sup> Interactions between valence and core electrons were described by norm conserving scalar relativistic pseudopotentials.<sup>44-46</sup> The Kohn-Sham orbitals were expanded in a plane-wave basis with a cutoff energy of 210 Ry, while a cutoff of 840 Ry was used for the charge density. The Brillouin zone (BZ) was sampled using a Gamma-centered  $18 \times 18 \times 3$  grid following the scheme proposed by Monkhorst-Pack.<sup>47</sup> The semi-classical transport coefficients were calculated applying the BoltzTraP code to a *ab initio* calculation with a Brillouin zone sampled with a Gamma-centered  $36 \times 36 \times 6$  grid following the scheme proposed by Monkhorst-Pack.<sup>48</sup>

## Results and Discussion

**Synthesis.** Our initial attempt to use CuO as a precursor in a  $\text{Na}_2\text{Se}_x$  flux was intended to synthesize possible analogs of  $\text{Na}_{1.9}\text{Cu}_2\text{Se}_2 \cdot \text{Cu}_2\text{O}$ .<sup>20</sup> After the  $\text{NaCu}_4\text{Se}_4$  compound was discovered, we conducted control experiments with flux reactions using CuO and Cu as the only copper source, i.e.,  $\text{Na}_2\text{Se}/\text{CuO}/\text{Se}$  and  $\text{Na}_2\text{Se}/\text{Cu}/\text{Se}$  mixtures in various elemental ratios and the same reaction conditions as described above. The reaction of  $\text{Na}_2\text{Se}/\text{CuO}/\text{Se}$  produced  $\text{NaCu}_4\text{Se}_4$ , but with low yield giving only a few small pieces. In contrast, the reaction of  $\text{Na}_2\text{Se}/\text{CuO}/\text{Cu}/\text{Se}$  gave  $\text{NaCu}_4\text{Se}_4$  with significantly increased yield. As for the reaction of  $\text{Na}_2\text{Se}/\text{Cu}/\text{Se}$ , it generated  $\text{NaCu}_6\text{Se}_4$  and  $\text{NaCuSe}$  as the products without any sign of  $\text{NaCu}_4\text{Se}_4$  formation.<sup>15</sup> Using the stoichiometry determined by EDS the X-ray single crystal diffraction analysis, we targeted  $\text{NaCu}_4\text{Se}_4$  by direct combination of elemental Na, Cu and Se in a 1:4:4 ratio, and heating this mixture to 873 K for 10 hr. However, this reaction resulted only in CuSe and NaCuSe as products, further confirming that oxide precursor is required for the synthesis of  $\text{NaCu}_4\text{Se}_4$ . We therefore conclude that the presence of CuO is crucial for the formation of  $\text{NaCu}_4\text{Se}_4$  in the  $\text{Na}_2\text{Se}_x$  flux. The reaction mechanism is unclear at present, but we speculate that CuO plays a role in transforming elemental starting materials to special intermediates that lead to the  $\text{NaCu}_4\text{Se}_4$  framework. The temperature-dependent in situ XRD technique (also known as “panoramic synthesis”) may help identify the intermediate stage clusters in molten  $\text{Na}_2\text{Se}_x$ , as reported in the K/Cu/S, K/Sn/S and Cs/Sn/P/Se systems.<sup>49-51</sup>

A typical hexagonal plate-like crystal of  $\text{NaCu}_4\text{Se}_4$ , with side length of  $\sim 300 \mu\text{m}$  and thickness of  $\sim 50 \mu\text{m}$ , is shown in Figure 1a. In DTA experiments,  $\text{NaCu}_4\text{Se}_4$  exhibits an endothermic peak at 613 K and two exothermic peaks around 590 K, corresponding to the



melting and crystallization events, respectively (Figure S1). PXRD of the ground post-DTA sample reveals multiple peaks which can be indexed to NaCuSe and CuSe, indicating that NaCu<sub>4</sub>Se<sub>4</sub> melts incongruently (Figure S2).

**Crystal Structure.** The structure of NaCu<sub>4</sub>Se<sub>4</sub> consists of infinite [Cu<sub>4</sub>Se<sub>4</sub>]<sup>-</sup> layers charge balanced by Na<sup>+</sup> ions (Figure 1b). The [Cu<sub>4</sub>Se<sub>4</sub>]<sup>-</sup> layer is comprised of two unique Cu atoms (Figure 1c): Cu(1) is coordinated by three Se(1) atoms in a bent trigonal planar geometry with a bond length of 2.359(1) Å (Figure 1d). Cu(2) is coordinated by one Se(1) and three Se(2) atoms, in a distorted tetrahedral geometry with bond lengths of 2.424(3) and 2.425(1) Å, respectively (Figure 1e). The structure contains [Se<sub>2</sub>]<sup>2-</sup> dimers with Se-Se distance of 2.363(3) Å (Figure 1f). The CuSe<sub>4</sub> tetrahedra are separated by Se dimers and sandwiched by Cu(1) atoms to form the layer. The Na<sup>+</sup> cations (Figure 1g) are six coordinated by Se atoms with Na-Se distance of 3.009(1) Å.

NaCu<sub>4</sub>Se<sub>4</sub> has a structure related to the binary CuSe. As shown in Figure 2a, the [Cu<sub>4</sub>Se<sub>4</sub>]<sup>-</sup> slabs in NaCu<sub>4</sub>Se<sub>4</sub> can be viewed as being constructed by a subunit sliced from CuSe (*P6<sub>3</sub>/mmc*). For the related 2D and mixed-valent phases NaCu<sub>4</sub>Se<sub>3</sub><sup>12</sup> and NaCu<sub>6</sub>Se<sub>4</sub><sup>15</sup>, a significant difference is that these two compounds are built entirely from CuSe<sub>4</sub> units with all Cu atoms tetrahedrally coordinated. An additional difference is the presence of Se-Se bonding in NaCu<sub>4</sub>Se<sub>4</sub> which is absent in NaCu<sub>4</sub>Se<sub>3</sub> and NaCu<sub>6</sub>Se<sub>4</sub>. The NaCu<sub>4</sub>Se<sub>3</sub><sup>12</sup> and NaCu<sub>6</sub>Se<sub>4</sub><sup>15</sup> can be formulated as (Na<sup>+</sup>)(Cu<sup>+</sup>)<sub>4</sub>(Se<sup>-</sup>)(Se<sup>2-</sup>)<sub>2</sub> and (Na<sup>+</sup>)(Cu<sup>+</sup>)<sub>6</sub>(Se<sup>-</sup>)(Se<sup>2-</sup>)<sub>3</sub>, respectively. The chemical formula of NaCu<sub>4</sub>Se<sub>4</sub>, however, can be better represented either by (Na<sup>+</sup>)(Cu<sup>+</sup>)<sub>3</sub>(Cu<sup>2+</sup>)(Se<sup>2-</sup>)<sub>2</sub>(Se<sub>2</sub>)<sup>2-</sup> or (Na<sup>+</sup>)(Cu<sup>+</sup>)<sub>4</sub>(Se<sup>2-</sup>)(Se<sup>-</sup>)(Se<sub>2</sub>)<sup>2-</sup> with mixed valent (Cu<sup>+</sup>/Cu<sup>2+</sup>)<sup>52-54</sup> or (Se<sup>2-</sup>/Se<sup>-</sup>).<sup>12, 15</sup>

To interrogate valence states of the atoms in NaCu<sub>4</sub>Se<sub>4</sub>, we used XPS. In the case of Na, only one binding energy of 1072.1 eV corresponding to Na<sup>+</sup> was observed (Figure 3a). The binding energies of 932.7 and 952.5 eV for Cu correspond to Cu<sup>+</sup> 2p<sub>3/2</sub> and 2p<sub>1/2</sub> core states, with no Cu<sup>2+</sup> satellite peaks observed (Figure 3b), confirming that NaCu<sub>4</sub>Se<sub>4</sub> contains only Cu<sup>+</sup>. The energy range for Se is shown in Figure 3c, where the observed binding energies 53.57 and 54.43 eV correspond to Se 3d<sub>5/2</sub> and 3d<sub>3/2</sub> core states. These are well fitted by three valence states (labelled A (53.53 and 54.39 eV), B (54.39 and 55.25 eV) and C (55.33 and 56.19 eV)), which suggests NaCu<sub>4</sub>Se<sub>4</sub> has three electronic environments for Se, with the corresponding bond strengths being: A < B < C. Because the bond strength is inversely proportional to the bond length, we assign the A, B and C corresponding to Cu(2)–Se (2.424(3) Å), Se(2)–Se(2) (2.363(3) Å), and Cu(1)–Se (2.359(1) Å) bonds, respectively. Therefore, the XPS results directly confirm that NaCu<sub>4</sub>Se<sub>4</sub> is a mixed-valent compound with electron deficiency on the Se atoms. The preferred chemical formula is thus (Na<sup>+</sup>)(Cu<sup>+</sup>)<sub>4</sub>(Se<sup>2-</sup>)(Se<sup>-</sup>)(Se<sub>2</sub>)<sup>2-</sup>. This implies the delocalized holes exist in the compound, generating a metallic system, similar to CuSe,<sup>55</sup> NaCu<sub>4</sub>S<sub>4</sub>,<sup>13</sup> and Na<sub>3</sub>Cu<sub>4</sub>S<sub>4</sub>.<sup>10</sup> However, as we will show below, the electronic structure calculations suggest the oxidation is actually more delocalized on both Cu as well as Se atoms.

**Charge Transport Properties.** The charge transport properties of NaCu<sub>4</sub>Se<sub>4</sub> were probed with resistivity and Hall effect measurements on a single crystal sample. Figure 4a shows the resistivity ( $\rho$ ) from 2 to 300 K along the plane of the single crystal.  $\rho$  decreases linearly with decreasing temperature, from  $1.17 \times 10^{-4}$   $\Omega$  cm at 300 K to  $2.22 \times 10^{-6}$   $\Omega$  cm at 20 K, indicating metallic behavior. The data between 2 and 20 K shows  $T^2$  dependence, which

can be fitted by the equation of  $\rho(T) = \rho_0 + AT^2$  with the residual resistivity  $\rho_0$  and constant  $A$  determined to be  $0.15 \mu\Omega \text{ cm}$  and  $0.0048 \mu\Omega \text{ cm/K}^2$ , respectively, suggestive of Fermi-liquid behavior.<sup>56</sup> Furthermore, the residual resistance ratio ( $RRR = \rho_{300\text{K}}/\rho_{2\text{K}}$ ) is  $\sim 424$ , indicating the high quality of the single crystal.

The carrier concentration ( $n$ ) and mobility ( $\mu$ ) in  $\text{NaCu}_4\text{Se}_4$  were determined by Hall effect measurements on the same single crystal used for resistivity. The Hall resistivity ( $\rho_{xy}$ ) exhibited a linear dependence on applied field (Figure S3).  $\rho_{xy}$  is positive for positive fields at all temperatures below 300 K, indicating that holes are the dominant charge carriers in  $\text{NaCu}_4\text{Se}_4$ . The  $n$  was calculated from the equation  $n = 1/(R_H e)$  where  $R_H$  denotes the Hall coefficient. As depicted in Figure 4b,  $n$  at room temperature is  $\sim 5.39 \times 10^{21} \text{ cm}^{-3}$  which is of the same order found for  $\text{NaCu}_4\text{Se}_3$  ( $\sim 6.12 \times 10^{21} \text{ cm}^{-3}$ ) and  $\text{NaCu}_6\text{Se}_4$  ( $\sim 2.83 \times 10^{21} \text{ cm}^{-3}$ ).<sup>12, 15</sup> This value decreases slightly to  $2.95 \times 10^{21} \text{ cm}^{-3}$  at 2 K. The  $\mu$ , estimated by the formula  $\mu = 1/(\rho n e)$ , is  $\sim 11 \text{ cm}^2 \text{ V}^{-1} \text{ s}^{-1}$  at room temperature, and remarkably increases by nearly two orders of magnitude to  $\sim 808 \text{ cm}^2 \text{ V}^{-1} \text{ s}^{-1}$  at 2 K (Figure 4c). In the range of 15 – 300 K, the  $\mu$  displays a  $T^{-3/2}$  dependence behavior, suggesting acoustic phonon scattering is occurring.<sup>57-58</sup> Below 15 K, hole mobility is roughly constant, suggesting a combination of impurity scattering and acoustic phonon scattering.<sup>57-58</sup> This mobility value is the highest among all metallic copper selenides. For example, at 2 K the mobilities are  $\sim 25 \text{ cm}^2 \text{ V}^{-1} \text{ s}^{-1}$  for  $\text{CuSe}$ <sup>59</sup>,  $\sim 6.5 \text{ cm}^2 \text{ V}^{-1} \text{ s}^{-1}$  for  $\text{NaCu}_4\text{S}_4$ <sup>13</sup>,  $\sim 1.9 \text{ cm}^2 \text{ V}^{-1} \text{ s}^{-1}$  for  $\text{NaCu}_4\text{Se}_3$ <sup>12</sup> and  $\sim 22 \text{ cm}^2 \text{ V}^{-1} \text{ s}^{-1}$  for  $\text{NaCu}_6\text{Se}_4$ <sup>15</sup>, comparison in Figure 4d.

To evaluate the Debye temperature ( $\Theta_D$ ) and effective mass ( $m^*$ ) of the holes in  $\text{NaCu}_4\text{Se}_4$ , the heat capacity ( $C$ ) was measured. As shown in Figure 5, according to the formula  $C(T) = \gamma T + \beta_1 T^3 + \beta_2 T^5$  in which  $\gamma T$  and  $\beta_1 T^3 + \beta_2 T^5$  are the electron and phonon

contributions, the calculated coefficients are  $\gamma = 6.8 \text{ mJ mol}^{-1} \text{ K}^{-2}$ ,  $\beta_1 = 2.8 \text{ mJ mol}^{-1} \text{ K}^{-4}$ , and  $\beta_2 = 0.0085 \text{ mJ mol}^{-1} \text{ K}^{-6}$ , respectively.<sup>39</sup>  $\Theta_D$ , calculated by  $\Theta_D = (12\pi^4NR/5\beta)^{1/3}$ , is determined to be  $\sim 140 \text{ K}$ .  $m^*$  is found to be  $\sim 3 m_0$ , as estimated by the relationship with  $\gamma = \pi^2/3\kappa_B^2N(E_F) = 1.36 \times 10^{-4} \times V_{\text{mol}}^{2/3}n_\gamma^{1/3}m^*/m_0$ ,<sup>40</sup> where  $V_{\text{mol}}$ ,  $n_\gamma$ , and  $m^*/m_0$  are molar volume, carrier concentration per atom, and effective mass. Compared with  $m^*$  in  $\text{KCu}_3\text{Se}_2$  ( $\sim 7.1 m_0$ )<sup>5</sup>, the value of  $m^*$  in  $\text{NaCu}_4\text{Se}_4$  is much smaller, which is consistent with the much higher mobility.

**Band Structure Calculations.** To gain a deeper understanding of this material, we performed first-principles electronic structure calculations. The band structure of  $\text{NaCu}_4\text{Se}_4$  has several bands crossing the Fermi level in the vicinity of the  $\Gamma$ -point, Figure 6. The Fermi surfaces show that the electrons are constrained in two-dimensions.

Figure 7a shows both the calculated total density of states (DOS) and the projected DOS (pDOS) for each atomic species in the vicinity of the Fermi level. Together with Figure 7b and 7c, it shows that the electronic behavior of  $\text{NaCu}_4\text{Se}_4$  is dominated by copper  $d$ -orbitals and selenium  $p$ -orbitals which contribute equally to the DOS at  $E_F$  (Figure S4).

From the *ab initio* calculation, we can estimate the (zero temperature) charge carrier concentration by simply integrating the density of states between the Fermi level and the top of the conduction bands. Such an estimate gives a charge carrier density of the order of  $\sim 5 \times 10^{21} \text{ cm}^{-3}$ , which agrees well with the experimental value from the Hall effect.

The charge carrier's density of states effective mass is given by  $m_{DOS}^* = \sqrt[3]{m_x^*m_y^*m_z^*}$ , where  $m_x^*$ ,  $m_y^*$ , and  $m_z^*$  stand for the effective masses along different directions in the Brillouin zone. This quantity can also be estimated from the *ab initio* results, by fitting it

to the density of states of a 3D isotropic parabolic dispersion, which can be related to an isotropic one,  $E_{\vec{k}'} = \frac{\hbar^2 \vec{k}'^2}{2m_{DOS}^*}$ , with the following transformation

$$\vec{k}' = \sqrt{m_{DOS}^*} \left( \frac{k_x}{\sqrt{m_x^*}}, \frac{k_y}{\sqrt{m_y^*}}, \frac{k_z}{\sqrt{m_z^*}} \right).$$

Such a procedure yields a charge carrier effective mass of  $\sim 2.2 m_0$  which is close to the experimental estimate based on the heat capacity data ( $\sim 3 m_0$ ). The close resemblance between the theory and experiments validates the convincing transport properties arising from the unique layered structure of NaCu<sub>4</sub>Se<sub>4</sub>. NaCu<sub>4</sub>Se<sub>4</sub> has a band structure which is very similar to the band structures of NaCu<sub>4</sub>Se<sub>3</sub><sup>12</sup> and NaCu<sub>6</sub>Se<sub>4</sub><sup>15</sup>. Herein, the high mobility in NaCu<sub>4</sub>Se<sub>4</sub> at 2 K possibly results from high crystallinity of the as-synthesized single crystal, as confirmed by the very large RRR.

**Magnetoresistance.** High carrier mobility in metals is associated with large MR, e.g., in the layered transition-metal dichalcogenide WTe<sub>2</sub><sup>21</sup> and graphite.<sup>60</sup> Considering the high mobility in NaCu<sub>4</sub>Se<sub>4</sub> and its 2D structure, we also investigated the MR in this material. When a magnetic field (0 – 9 T) is applied perpendicular to the direction of the current flow (Figure 8a), the resistivity of NaCu<sub>4</sub>Se<sub>4</sub> shows substantial increase in a temperature range 2 – 50 K, indicating large positive MR. The field dependence of MR at various temperatures is shown in Figure 8b and 8c. All MR exhibits linear behavior showing no sign of saturation up to 9 T. A maximum MR of  $\sim 1400\%$  was obtained at 9 T and 2 K, a value which qualifies as giant.<sup>61</sup> The MR values decrease with increasing temperature: for an applied magnetic field of 9 T, from  $\sim 1400\%$  at 2 K to  $\sim 10\%$  at 50 K which reflects the large drop in mobility with rising temperature, Figure 8d.

To probe the anisotropy of MR, the angle dependence on the same single crystal of  $\text{NaCu}_4\text{Se}_4$  was measured using the sample rotator on PPMS from  $0 - 360^\circ$ . Figure 9a shows the field dependence of the MR with different angles between the applied magnetic field and the crystallographic  $c$  axis ( $0^\circ$ ,  $30^\circ$ ,  $60^\circ$  and  $90^\circ$ ). The MR maximizes at  $0^\circ$  and decreases when the applied magnetic field gradually tilts away from the  $c$  axis. When it arrives at  $90^\circ$  where the magnetic field is applied in plane, MR shows a linear behavior with a sign of saturation at large magnetic fields and its value is much smaller: the MR at 9 T at 2 K ( $\sim 280\%$ ) is approximately five times smaller than that measured at  $0^\circ$ . The angle-dependent MR data at 2 K with the applied magnetic field of 9 T could be well fitted with the function of  $|\cos(\theta)|$  as shown in Figure 9b. This clearly indicates high anisotropy where the carriers' movement is 2D constrained in planes perpendicular to the crystallographic  $c$  axis.<sup>62-63</sup>

Generally, positive, nonsaturating and linear MR can be attributed to one of three origins. One is that electrons move in a polycrystalline sample with an open Fermi surface, as reported in the  $\text{Ag}_2\text{Q}$  ( $\text{Q} = \text{Se}, \text{Te}$ ) semiconductors.<sup>22-23</sup> While  $\text{NaCu}_4\text{Se}_4$  has an open Fermi surface, our measurement is on a high-quality single crystal. As a consequence, this is likely not the source of the linear MR observed in this compound. Another case is the extreme quantum limit where one Landau level dominates, which has inspired extensive interest in some quantum materials with Dirac points, such as  $\text{SrMnBi}_2$ ,<sup>64</sup>  $\text{SrMnSb}_2$ ,<sup>65</sup>  $\text{TaAs}$ ,<sup>29, 66</sup> and  $\text{ZrSiS}$ .<sup>30</sup> In this case, the MR usually exhibits a crossover at a critical field  $B^*$  from a semiclassical weak-field  $B^2$  dependence to the high-field linear-field dependence.<sup>67</sup> Considering the calculated band structure of  $\text{NaCu}_4\text{Se}_4$ , we can exclude this case because no apparent Dirac point is present in  $\text{NaCu}_4\text{Se}_4$ . We therefore suspect that the

linear MR in NaCu<sub>4</sub>Se<sub>4</sub> may be associated with the high mobility, as the third case.<sup>27</sup> From the transport data, both of the  $\mu$  and the MR simultaneously decrease dramatically with increasing temperature from 2 K to 50 K, which further confirms the link between  $\mu$  and MR in NaCu<sub>4</sub>Se<sub>4</sub>.

## Conclusions

It is not often that a new unique synthesis is discovered where the use of a particular precursor leads to a new compound. This is especially remarkable when this occurs in a composition space which is already very congested with other related compounds. The introduction of CuO as the metal source in reactive NaSe<sub>x</sub> flux, enables a reaction route to the new 2D hexagonal compound NaCu<sub>4</sub>Se<sub>4</sub>. When CuO is not used, the reaction leads to other structurally related ternary Na/Cu/Se phases with no trace of NaCu<sub>4</sub>Se<sub>4</sub>. Therefore, the choice of unconventional precursors can, in some instances, alter the mechanism and stabilize reaction intermediates that lead to difficult to access phases. The newly formed metallic phase of layered NaCu<sub>4</sub>Se<sub>4</sub>, despite its very large hole concentration of  $\sim 10^{21}$  cm<sup>-3</sup>, features a high in-plane hole mobility of  $\sim 808$  cm<sup>2</sup>V<sup>-1</sup>s<sup>-1</sup> at 2 K, resulting in a correspondingly uncharacteristic nonsaturating giant MR of  $\sim 1400\%$  that remains linear up to 9 T. Given that NaCu<sub>4</sub>Se<sub>4</sub> is not a semimetal, at this point it is not clear if the nonsaturating giant MR in this material is due to a unique feature in the nature of electronic Fermi surface, or to some electronic inhomogeneity in the sample or even a new mechanism. Elucidating this question will require additional experiments including measurements at even high magnetic fields.

## ASSOCIATED CONTENT

**Supporting Information.** Experimental details for PXRD, SEM-EDS, and DTA, element ratios from EDS measurement, DTA results. PXRD patterns for NaCu<sub>4</sub>Se<sub>4</sub> before and after DTA measurements, Hall resistivity ( $\rho_{xy}$ ) at different temperatures (2 – 300 K), calculated projected density of states and band structure, and calculated temperature-dependent Seebeck coefficients for undoped, hole-doped, and electron-doped NaCu<sub>4</sub>Se<sub>4</sub> (PDF). Crystallographic data for NaCu<sub>4</sub>Se<sub>4</sub> (NaCu4Se4.cif) (CIF)

## AUTHOR INFORMATION

### Corresponding Author

\*E-mail: m-kanatzidis@northwestern.edu

### Author Contributions

The authors declare no competing financial interest.

### Acknowledgements

Research at Argonne primarily was supported by the U.S. Department of Energy, Office of Science, Basic Energy Sciences, Materials Sciences and Engineering Division. Computational resources utilized in first-principles calculations were provided by the University of Illinois Campus Cluster and the Center for Advanced 2D Materials Cluster in Singapore. SEM-EDS work was performed by use of the EPIC, Keck-II, and/or SPID facility(ies) of Northwestern University's NUANCE Center, which has received support from the Soft and Hybrid Nanotechnology Experimental (SHyNE) Resource (NSF ECCS-



1542205); the MRSEC program (NSF DMR-1121262) at the Materials Research Center; the International Institute for Nanotechnology (IIN); the Keck Foundation; and the State of Illinois, through the IIN.

## References

1. Lee, K. S.; Seo, D. K.; Whangbo, M. H.; Li, H.; Mackay, R.; Hwu, S. J., Vacancy ordering as the cause for the electrical resistivity anomalies and superlattice modulations in  $\text{ACu}_{7-x}\text{S}_4$  (A = Tl, K, Rb). *Journal of Solid State Chemistry* **1997**, *134* (1), 5-9.
2. Fleming, R. M.; Ter Haar, L. W.; DiSalvo, F. J., X-ray scattering study of charge-density waves in  $\text{K}_3\text{Cu}_8\text{S}_6$ . *Physical Review B* **1987**, *35* (10), 5388.
3. Sato, H.; Kojima, N.; Suzuki, K.; Enoki, T., Effects of alkali substitution and pressure on the charge-density wave transitions of two-dimensional metals  $\text{K}_3\text{Cu}_8\text{S}_6$  and  $\text{Rb}_3\text{Cu}_8\text{S}_6$ . *Journal of the Physical Society of Japan* **1993**, *62* (2), 647-658.
4. Kuo, Y. K.; Skove, M. J.; Verebelyi, D. T.; Li, H.; Mackay, R.; Hwu, S. J.; Whangbo, M. H.; Brill, J. W., Unusual physical properties of  $\text{KCu}_{7-x}\text{S}_4$  at diffusive one-dimensional ordering transitions. *Physical Review B* **1998**, *57* (6), 3315.
5. Rettie, A. J. E.; Sturza, M.; Malliakas, C. D.; Botana, A. S.; Chung, D. Y.; Kanatzidis, M. G., Copper vacancies and heavy holes in the two-dimensional semiconductor  $\text{KCu}_{3-x}\text{Se}_2$ . *Chemistry of Materials* **2017**, *29* (14), 6114-6121.
6. Dai, S.; Xi, Y.; Hu, C. G.; Liu, J. L.; Zhang, K. Y.; Yue, X. L.; Cheng, L.,  $\text{KCu}_7\text{S}_4$  nanowires and the Mn/ $\text{KCu}_7\text{S}_4$  nanostructure for solid-state supercapacitors. *Journal of Materials Chemistry A* **2013**, *1* (48), 15530-15534.
7. Dai, S. g.; Xu, W. N.; Xi, Y.; Wang, M. J.; Gu, X.; Guo, D. L.; Hu, C. G., Charge storage in  $\text{KCu}_7\text{S}_4$  as redox active material for a flexible all-solid-state supercapacitor. *Nano Energy* **2016**, *19*, 363-372.
8. Hull, S., Superionics: crystal structures and conduction processes. *Reports on Progress in Physics* **2004**, *67* (7), 1233-1314.
9. Burschka, C.,  $\text{Na}_3\text{Cu}_4\text{S}_4$ -ein thiocuprat mit unverknüpften  $^{1\infty}[\text{Cu}_4\text{S}_4]$ -Ketten/ $\text{Na}_3\text{Cu}_4\text{S}_4$ -a thiocuprate with isolated  $^{1\infty}[\text{Cu}_4\text{S}_4]$ -chains. *Zeitschrift für Naturforschung B* **1979**, *34* (3), 396-397.
10. Peplinski, Z.; Brown, D. B.; Watt, T.; Hatfield, W. E.; Day, P., Electrical properties of sodium copper sulfide ( $\text{Na}_3\text{Cu}_4\text{S}_4$ ), a mixed-valence one-dimensional metal. *Inorganic Chemistry* **1982**, *21* (5), 1752-1755.
11. Brown, D. B.; Zubieta, J. A.; Vella, P. A.; Wroblewski, J. T.; Watt, T.; Hatfield, W. E.; Day, P., Solid-state structure and electronic properties of a mixed-valence two-dimensional metal, potassium copper sulfide ( $\text{KCu}_4\text{S}_3$ ). *Inorganic Chemistry* **1980**, *19* (7), 1945-1950.
12. Sturza, M.; Bugaris, D. E.; Malliakas, C. D.; Han, F.; Chung, D. Y.; Kanatzidis, M. G., Mixed-valent  $\text{NaCu}_4\text{Se}_3$ : a two-dimensional metal. *Inorganic Chemistry* **2016**, *55* (10), 4884-4890.
13. Zhang, X.; Kanatzidis, M. G.; Hogan, T.; Kannewurf, C. R.,  $\text{NaCu}_4\text{S}_4$ , a simple new low-dimensional, metallic copper polychalcogenide, structurally related to  $\text{CuS}$ . *Journal of the American Chemical Society* **1996**, *118* (3), 693-694.
14. Zhang, X.; Park, Y.; Hogan, T.; Schindler, J. L.; Kannewurf, C. R.; Seong, S.; Albright, T.; Kanatzidis, M. G., Reactivity of copper in molten polytelluride salts.  $\text{K}_4\text{Cu}_8\text{Te}_{11}$ ,  $\text{A}_3\text{Cu}_8\text{Te}_{10}$  (A = Rb, Cs),  $\text{AA}'_2\text{Cu}_8\text{Te}_{10}$  (A, A' = K, Rb, Cs), and  $\text{A}_2\text{BaCu}_8\text{Te}_{10}$  (A = K, Rb, Cs): novel solids based on endohedrally occupied  $[\text{Cu}_8\text{Te}_{12}]$  dodecahedral cage-clusters. *Journal of the American Chemical Society* **1995**, *117* (41), 10300-10310.

15. Sturza, M.; Malliakas, C. D.; Bugaris, D. E.; Han, F.; Chung, D. Y.; Kanatzidis, M. G., NaCu<sub>6</sub>Se<sub>4</sub>: a layered compound with mixed valency and metallic properties. *Inorganic Chemistry* **2014**, *53* (22), 12191-12198.
16. Berger, R.; Van Bruggen, C. F., TiCu<sub>2</sub>Se<sub>2</sub>: a p-type metal with a layer structure. *Journal of the Less Common Metals* **1984**, *99* (1), 113-123.
17. Huai, W. J.; Shen, J. N.; Lin, H.; Chen, L.; Wu, L. M., Electron-deficient telluride Cs<sub>3</sub>Cu<sub>20</sub>Te<sub>13</sub> with sodalite-type network: syntheses, structures, and physical properties. *Inorganic Chemistry* **2014**, *53* (11), 5575-5580.
18. Kanatzidis, M. G.; Sutorik, A. C., The application of polychalcogenide salts to the exploratory synthesis of solid state multinary chalcogenides at intermediate temperatures. *Progress in Inorganic Chemistry* **1995**, 151-265.
19. Kanatzidis, M. G., Discovery-Synthesis, Design, and Prediction of Chalcogenide Phases. *Inorg. Chem.* **2017**, *56* (6), 3158-3173.
20. Park, Y.; DeGroot, D. C.; Schindler, J. L.; Kannewurf, C. R.; Kanatzidis, M. G., Intergrowth of two different layered networks in the metallic copper oxyselenide Na<sub>1-9</sub>Cu<sub>2</sub>Se<sub>2</sub>.Cu<sub>2</sub>O. *Chemistry of Materials* **1993**, *5* (1), 8-10.
21. Ali, M. N.; Xiong, J.; Flynn, S.; Tao, J.; Gibson, Q. D.; Schoop, L. M.; Liang, T.; Haldolaarachchige, N.; Hirschberger, M.; Ong, N., Large, non-saturating magnetoresistance in WTe<sub>2</sub>. *Nature* **2014**, *514* (7521), 205-208.
22. Lee, M.; Rosenbaum, T.; Saboungi, M.-L.; Schnyders, H., Band-gap tuning and linear magnetoresistance in the silver chalcogenides. *Physical Review Letters* **2002**, *88* (6), 066602.
23. Xu, R.; Husmann, A.; Rosenbaum, T.; Saboungi, M.-L.; Enderby, J.; Littlewood, P., Large magnetoresistance in non-magnetic silver chalcogenides. *Nature* **1997**, *390* (6655), 57-60.
24. Zhang, W.; Yu, R.; Feng, W.; Yao, Y.; Weng, H.; Dai, X.; Fang, Z., Topological Aspect and Quantum Magnetoresistance of β-Ag<sub>2</sub>Te. *Physical Review Letters* **2011**, *106* (15), 156808.
25. Liu, Z.; Zhou, B.; Zhang, Y.; Wang, Z.; Weng, H.; Prabhakaran, D.; Mo, S.-K.; Shen, Z.; Fang, Z.; Dai, X., Discovery of a three-dimensional topological Dirac semimetal, Na<sub>3</sub>Bi. *Science* **2014**, *343* (6173), 864-867.
26. Xiong, J.; Kushwaha, S. K.; Liang, T.; Krizan, J. W.; Hirschberger, M.; Wang, W.; Cava, R.; Ong, N., Evidence for the chiral anomaly in the Dirac semimetal Na<sub>3</sub>Bi. *Science* **2015**, *350* (6259), 413-416.
27. Narayanan, A.; Watson, M.; Blake, S. F.; Bruyant, N.; Drigo, L.; Chen, Y. L.; Prabhakaran, D.; Yan, B.; Felser, C.; Kong, T., Linear magnetoresistance caused by mobility fluctuations in n-doped Cd<sub>3</sub>As<sub>2</sub>. *Physical Review Letters* **2015**, *114* (11), 117201.
28. Shekhar, C.; Nayak, A. K.; Sun, Y.; Schmidt, M.; Nicklas, M.; Leermakers, I.; Zeitler, U.; Skourski, Y.; Wosnitza, J.; Liu, Z., Extremely large magnetoresistance and ultrahigh mobility in the topological Weyl semimetal candidate NbP. *Nature Physics* **2015**, *11* (8), 645-649.
29. Yang, L.; Liu, Z.; Sun, Y.; Peng, H.; Yang, H.; Zhang, T.; Zhou, B.; Zhang, Y.; Guo, Y.; Rahn, M., Weyl semimetal phase in the non-centrosymmetric compound TaAs. *Nature Physics* **2015**, *11* (9), 728-732.

30. Singha, R.; Pariari, A. K.; Satpati, B.; Mandal, P., Large nonsaturating magnetoresistance and signature of nondegenerate Dirac nodes in ZrSiS. *Proceedings of the National Academy of Sciences* **2017**, *114* (10), 2468-2473.
31. Hosen, M. M.; Dimitri, K.; Belopolski, I.; Maldonado, P.; Sankar, R.; Dhakal, N.; Dhakal, G.; Cole, T.; Oppeneer, P. M.; Kaczorowski, D., Tunability of the topological nodal-line semimetal phase in ZrSiX-type materials (X = S, Se, Te). *Physical Review B* **2017**, *95* (16), 161101.
32. Leahy, I. A.; Lin, Y.-P.; Siegfried, P. E.; Treglia, A. C.; Song, J. C.; Nandkishore, R. M.; Lee, M., Non-saturating large magnetoresistance in semimetals. *Proceedings of the National Academy of Sciences* **2018**, *115* (42), 10570-10575.
33. Chung, I.; Biswas, K.; Song, J. H.; Androulakis, J.; Chondroudis, K.; Paraskevopoulos, K. M.; Freeman, A. J.; Kanatzidis, M. G., Rb<sub>4</sub>Sn<sub>5</sub>P<sub>4</sub>Se<sub>20</sub>: a semimetallic selenophosphate. *Angewandte Chemie International Edition* **2011**, *50* (38), 8834-8838.
34. Chung, I.; Song, J. H.; Jang, J. I.; Freeman, A. J.; Kanatzidis, M. G., Na<sub>2</sub>Ge<sub>2</sub>Se<sub>5</sub>: a highly nonlinear optical material. *Journal of Solid State Chemistry* **2012**, *195*, 161-165.
35. X-RED; X.-A. X.-S., *STOE & Cie GmbH: Darmstadt, Germany* **2009**.
36. Sheldrick, G. M., A short history of SHELX. *Acta Crystallographica Section A: Foundations of Crystallography* **2007**, *64* (1), 112-122.
37. Baibich, M. N.; Broto, J. M.; Fert, A.; Van Dau, F. N.; Petroff, F.; Etienne, P.; Creuzet, G.; Friederich, A.; Chazelas, J., Giant magnetoresistance of (001)Fe/(001)Cr magnetic superlattices. *Physical Review Letters* **1988**, *61* (21), 2472.
38. Moritomo, Y.; Asamitsu, A.; Kuwahara, H.; Tokura, Y., Giant magnetoresistance of manganese oxides with a layered perovskite structure. *Nature* **1996**, *380* (6570), 141-144.
39. Chen, H. J.; Claus, H.; Bao, J. K.; Stoumpos, C. C.; Chung, D. Y.; Kwok, W. K.; Kanatzidis, M. G., Superconductivity and structural conversion with Na and K doping of the narrow-gap semiconductor CsBi<sub>4</sub>Te<sub>6</sub>. *Chemistry of Materials* **2018**, *30* (15), 5293-5304.
40. Gopal, E., Specific heat at low temperatures heywood. London: 1966.
41. Kohn, W.; Sham, L. J., Self-Consistent Equations Including Exchange and Correlation Effects. *Phys. Rev.* **1965**, *140*, A1133.
42. Giannozzi, P.; Baroni, S.; Bonini, N.; Calandra, M.; Car, R.; Cavazzoni, C.; Ceresoli, D.; Chiarotti, G. L.; Cococcioni, M.; Dabo, I., QUANTUM ESPRESSO: a modular and open-source software project for quantum simulations of materials. *Journal of Physics: Condensed Matter* **2009**, *21* (39), 395502.
43. Perdew, J. P.; Burke, K.; Ernzerhof, M., Generalized gradient approximation made simple. *Physical Review Letters* **1996**, *77* (18), 3865.
44. Troullier, N.; Martins, J. L., Efficient pseudopotentials for plane-wave calculations. *Physical Review B* **1991**, *43* (3), 1993.
45. Goedecker, S.; Teter, M.; Hutter, J., Separable dual-space Gaussian pseudopotentials. *Physical Review B* **1996**, *54* (3), 1703.
46. Hartwigsen, C.; Goedecker, S.; Hutter, J., Relativistic separable dual-space Gaussian pseudopotentials from H to Rn. *Physical Review B* **1998**, *58* (7), 3641.
47. Monkhorst, H. J.; Pack, J. D., Special points for Brillouin-zone integrations. *Physical Review B* **1976**, *13* (12), 5188.

48. Madsen, G. K.; Singh, D. J., BoltzTraP. A code for calculating band-structure dependent quantities. *Computer Physics Communications* **2006**, *175* (1), 67-71.
49. Shoemaker, D. P.; Hu, Y.-J.; Chung, D. Y.; Halder, G. J.; Chupas, P. J.; Soderholm, L.; Mitchell, J.; Kanatzidis, M. G., In situ studies of a platform for metastable inorganic crystal growth and materials discovery. *Proceedings of the National Academy of Sciences* **2014**, *111* (30), 10922-10927.
50. Shoemaker, D. P.; Chung, D. Y.; Mitchell, J.; Bray, T. H.; Soderholm, L.; Chupas, P. J.; Kanatzidis, M. G., Understanding fluxes as media for directed synthesis: In situ local structure of molten potassium polysulfides. *Journal of the American Chemical Society* **2012**, *134* (22), 9456-9463.
51. Haynes, A. S.; Stoumpos, C. C.; Chen, H.; Chica, D.; Kanatzidis, M. G., Panoramic synthesis as an effective materials discovery tool: The system Cs/Sn/P/Se as a test case. *Journal of the American Chemical Society* **2017**, *139* (31), 10814-10821.
52. Bednorz, J. G.; Müller, K. A., Possible high T<sub>c</sub> superconductivity in the Ba-La-Cu-O system. *Zeitschrift für Physik B Condensed Matter* **1986**, *64* (2), 189-193.
53. Wu, M.-K.; Ashburn, J. R.; Torng, C.; Hor, P. H.; Meng, R. L.; Gao, L.; Huang, Z. J.; Wang, Y.; Chu, a., Superconductivity at 93 K in a new mixed-phase Y-Ba-Cu-O compound system at ambient pressure. *Physical Review Letters* **1987**, *58* (9), 908.
54. Mazin, I., Structural and electronic properties of the two-dimensional superconductor CuS with 1 1 3-valent copper. *Physical Review B* **2012**, *85* (11), 115133.
55. Krill, G.; Panissod, P.; Lapierre, M. F.; Gautier, F.; Robert, C.; Eddine, M. N., Magnetic properties and phase transitions of the metallic CuX<sub>2</sub> dichalcogenides (X = S, Se, Te) with pyrite structure. *Journal of Physics C: Solid State Physics* **1976**, *9* (8), 1521-1533.
56. Chen, H. J.; Narayan, A.; Stoumpos, C. C.; Zhao, J.; Han, F.; Chung, D. Y.; Wagner, L. K.; Kwok, W. K.; Kanatzidis, M. G., Semiconducting Ba<sub>3</sub>Sn<sub>3</sub>Sb<sub>4</sub> and metallic Ba<sub>7-x</sub>Sn<sub>11</sub>Sb<sub>15-y</sub> (x = 0.4, y = 0.6) Zintl phases. *Inorganic Chemistry* **2017**, *56* (22), 14251-14259.
57. Zheng, G.; Su, X.; Xie, H.; Shu, Y.; Liang, T.; She, X.; Liu, W.; Yan, Y.; Zhang, Q.; Uher, C., High thermoelectric performance of p-BiSbTe compounds prepared by ultra-fast thermally induced reaction. *Energy & Environmental Science* **2017**, *10* (12), 2638-2652.
58. Zheng, Z.; Su, X.; Deng, R.; Stoumpos, C. C.; Xie, H.; Liu, W.; Yan, Y.; Hao, S.; Uher, C.; Wolverton, C., Rhombohedral to Cubic Conversion of GeTe via MnTe alloying Leads to Ultralow Thermal Conductivity, Electronic Band Convergence and High Thermoelectric Performance. *Journal of the American Chemical Society* **2018**, *140* (7) 2673-2686.
59. Ogorelec, Z.; Selinger, D., Some electrical properties of synthetic klockmannite, CuSe. *Journal of Materials Science* **1971**, *6* (2), 136-139.
60. Soule, D., Magnetic field dependence of the Hall effect and magnetoresistance in graphite single crystals. *Physical Review* **1958**, *112* (3), 698.
61. Tafti, F.; Gibson, Q.; Kushwaha, S.; Haldolaarachchige, N.; Cava, R., Resistivity plateau and extreme magnetoresistance in LaSb. *Nature Physics* **2016**, *12* (3), 272-277.
62. Pippard, A. B., *Magnetoresistance in metals*. Cambridge University Press: 1989; Vol. 2.

63. Qu, D. X.; Hor, Y. S.; Xiong, J.; Cava, R. J.; Ong, N. P., Quantum oscillations and Hall anomaly of surface states in the topological insulator  $\text{Bi}_2\text{Te}_3$ . *Science* **2010**, *329* (5993), 821-824.
64. Park, J.; Lee, G.; Wolff-Fabris, F.; Koh, Y.; Eom, M.; Kim, Y.; Farhan, M.; Jo, Y.; Kim, C.; Shim, J. H., Anisotropic Dirac fermions in a Bi square net of  $\text{SrMnBi}_2$ . *Physical Review Letters* **2011**, *107* (12), 126402.
65. Liu, J.; Hu, J.; Zhang, Q.; Graf, D.; Cao, H. B.; Radmanesh, S.; Adams, D.; Zhu, Y.; Cheng, G.; Liu, X., A magnetic topological semimetal  $\text{Sr}_{1-y}\text{Mn}_{1-z}\text{Sb}_2$  ( $y, z < 0.1$ ). *Nature Materials* **2017**, *16* (9), 905-910.
66. Xu, S.-Y.; Belopolski, I.; Alidoust, N.; Neupane, M.; Bian, G.; Zhang, C. L.; Sankar, R.; Chang, G.; Yuan, Z.; Lee, C. C., Discovery of a Weyl fermion semimetal and topological Fermi arcs. *Science* **2015**, *349* (6248), 613-617.
67. Wang, K.; Graf, D.; Lei, H.; Tozer, S. W.; Petrovic, C., Quantum transport of two-dimensional Dirac fermions in  $\text{SrMnBi}_2$ . *Physical Review B* **2011**, *84* (22), 220401.

**Table 1.** Crystal data and structure refinement for NaCu<sub>4</sub>Se<sub>4</sub> at 293(2) K<sup>a</sup>

Empirical formula	NaCu <sub>4</sub> Se <sub>4</sub>
Formula weight	592.99
Temperature	293(2) K
Wavelength	0.71073 Å
Crystal system	hexagonal
Space group	<i>P</i> 6 <sub>3</sub> / <i>mmc</i>
Unit cell dimensions	$a = 3.9931(6)$ Å, $\alpha = 90^\circ$ $b = 3.9931(6)$ Å, $\beta = 90^\circ$ $c = 25.167(5)$ Å, $\gamma = 120^\circ$
Volume	347.52(13) Å <sup>3</sup>
<i>Z</i>	2
Density (calculated)	5.667 g/cm <sup>3</sup>
Absorption coefficient	32.963 mm <sup>-1</sup>
<i>F</i> (000)	526
Crystal size	0.634 × 0.455 × 0.104 mm <sup>3</sup>
$\theta$ range for data collection	3.238 to 29.055°
Index ranges	$-5 \leq h \leq 4$ , $-4 \leq k \leq 4$ , $-34 \leq l \leq 34$
Reflections collected	1949
Independent reflections	226 [ <i>R</i> <sub>int</sub> = 0.1202]
Completeness to $\theta = 25.242^\circ$	99.4%
Refinement method	Full-matrix least-squares on <i>F</i> <sup>2</sup>
Data / restraints / parameters	226 / 0 / 16
Goodness-of-fit	1.315
Final <i>R</i> indices [ <i>I</i> > 2σ( <i>I</i> )]	<i>R</i> <sub>obs</sub> = 0.0724, <i>wR</i> <sub>obs</sub> = 0.1351
<i>R</i> indices [all data]	<i>R</i> <sub>all</sub> = 0.0789, <i>wR</i> <sub>all</sub> = 0.1385
Extinction coefficient	0.0061(19)
Largest diff. peak and hole	1.889 and -1.164 e <sup>-</sup> ·Å <sup>-3</sup>

<sup>a</sup> $R = \Sigma||F_o| - |F_c||/\Sigma|F_o|$ ,  $wR = [\Sigma[w(|F_o|^2 - |F_c|^2)^2]/\Sigma[w(|F_o|^4)]]^{1/2}$ , and calculated  $w = 1/[\sigma^2(F_o^2) + (0.0419P)^2 + 11.4289P]$ , where  $P = (F_o^2 + 2F_c^2)/3$ .

**Table 2.** Atomic coordinates ( $\times 10^4$ ) and equivalent isotropic displacement parameters ( $\text{\AA}^2 \times 10^3$ ) for NaCu<sub>4</sub>Se<sub>4</sub> at 293(2) K with estimated standard deviations in parentheses.

Label	<i>x</i>	<i>y</i>	<i>z</i>	Occupancy	$U_{\text{eq}}^*$
Se(1)	3333	-3333	768(1)	1	14(1)
Se(2)	0	0	2030(1)	1	15(1)
Cu(2)	3333	-3333	1732(2)	1	20(1)
Cu(1)	6667	3333	968(2)	1	29(1)
Na(1)	0	0	0	1	21(3)

\* $U_{\text{eq}}$  is defined as one third of the trace of the orthogonalized  $U_{ij}$  tensor.

**Table 3.** Anisotropic displacement parameters ( $\text{\AA}^2 \times 10^3$ ) for NaCu<sub>4</sub>Se<sub>4</sub> at 293(2) K with estimated standard deviations in parentheses.

Label	$U_{11}$	$U_{22}$	$U_{33}$	$U_{12}$	$U_{13}$	$U_{23}$
Se(1)	9(1)	9(1)	23(1)	5(1)	0	0
Se(2)	12(1)	12(1)	21(1)	6(1)	0	0
Cu(2)	17(1)	17(1)	25(2)	8(1)	0	0
Cu(1)	18(2)	18(2)	50(2)	9(1)	0	0
Na(1)	18(4)	18(4)	28(6)	9(2)	0	0

The anisotropic displacement factor exponent takes the form:  $-2\pi^2[h^2a^{*2}U_{11} + \dots + 2hka^*b^*U_{12}]$ .

**Table 4.** Bond lengths [ $\text{\AA}$ ] and bond angles [ $^\circ$ ] for NaCu<sub>4</sub>Se<sub>4</sub> at 293(2) K with estimated standard deviations in parentheses.

Cu(1)-Se(1)	2.359(1)	Cu(2)-Se(2)	2.425(1)
Cu(2)-Se(1)	2.424(3)	Se(2)-Se(2)	2.363(3)
Na(1)-Se(1)	3.009(1)	Se(1)-Cu(1)-Se(1) ( $\times 3$ )	115.62(7)
Se(2)-Cu(2)-Se(2) ( $\times 3$ )	110.84(7)	Se(1)-Cu(2)-Se(2) ( $\times 3$ )	108.07(8)



## Figures

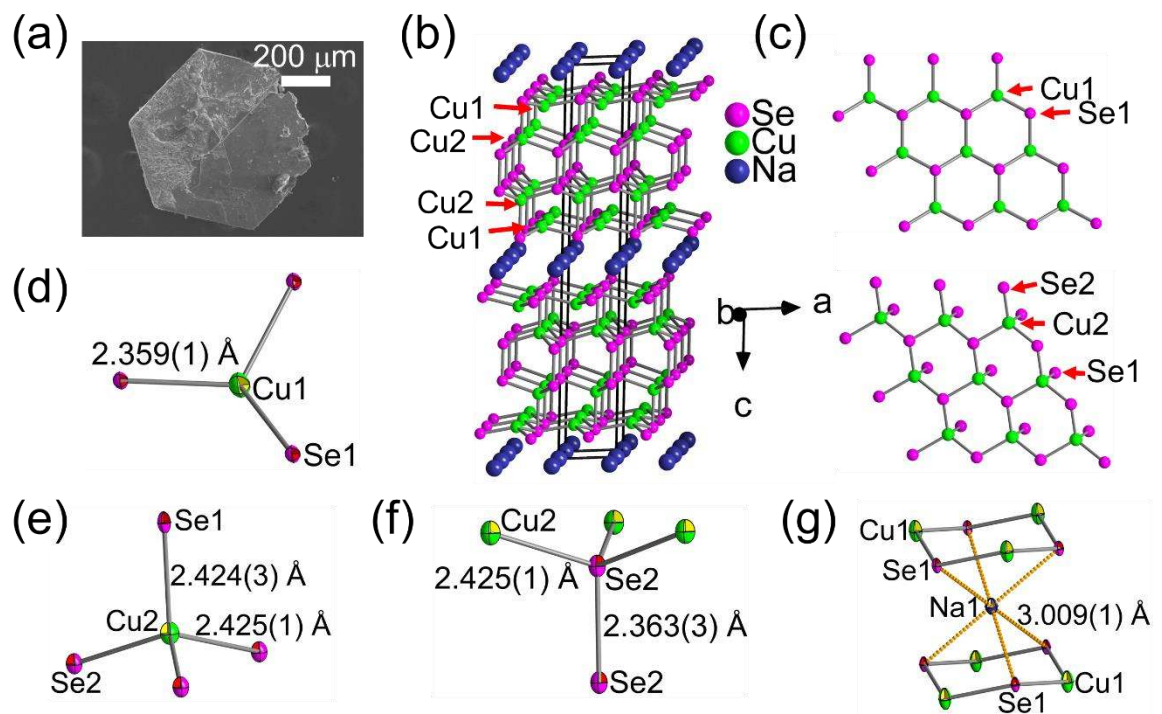


**Figure 1.** (a) SEM image of a typical NaCu<sub>4</sub>Se<sub>4</sub> crystal. (b) Crystal structure of NaCu<sub>4</sub>Se<sub>4</sub>. Na atoms are indigo, Cu atoms are green and Se atoms are pink. (c) Cu(1)-Se(1) and Cu(2)-Se(2) sublayers. Coordinated environments and bond distances of (d) Cu(1), (e) Cu(2), (f) Se(2), and (g) Na atoms.

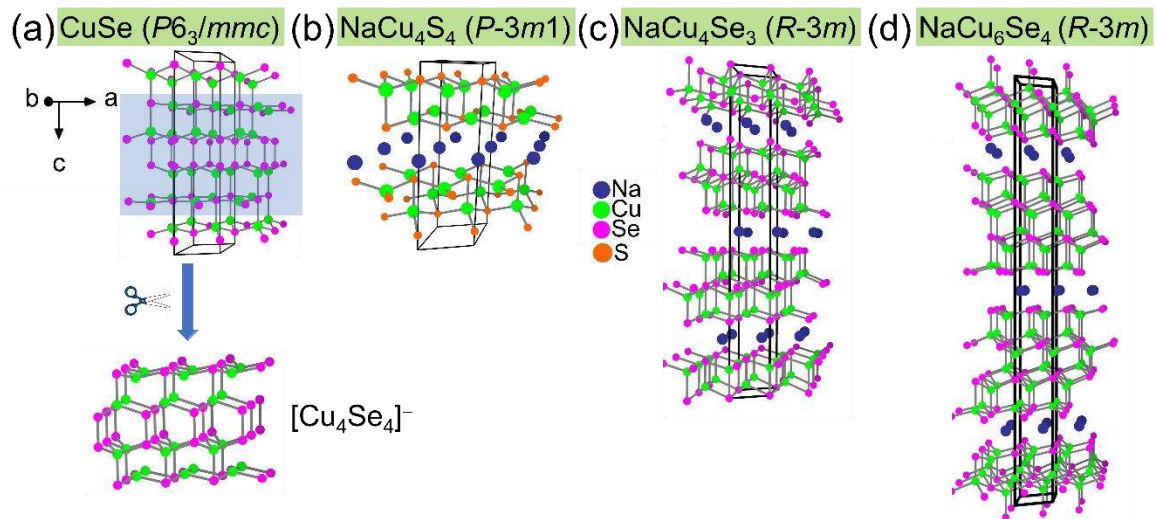


**Figure 2.** Comparison of the structure for  $\text{NaCu}_4\text{Se}_4$  with (a)  $\text{CuSe}$ , (b)  $\text{NaCu}_4\text{S}_4$ ,<sup>13</sup> (c)  $\text{NaCu}_4\text{Se}_3$ <sup>12</sup> and (d)  $\text{NaCu}_6\text{Se}_4$ <sup>15</sup> viewed along the crystallographic  $b$ -axis. Na atoms are indigo, Cu atoms are green, Se atoms are pink and S atoms are orange.

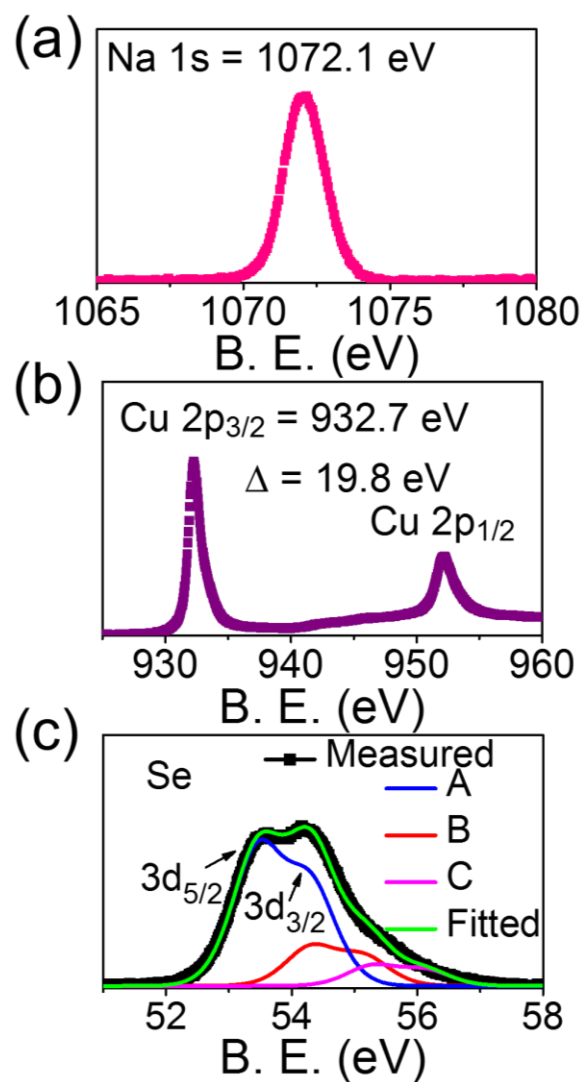


**Figure 3.** X-ray photoemission spectra of (a) Na 1s, (b) Cu 2p<sub>3/2</sub>, 2p<sub>1/2</sub>, and (c) Se 3d<sub>5/2</sub>, 3d<sub>3/2</sub> core states in NaCu<sub>4</sub>Se<sub>4</sub> (measured results, black line; fitted results, green line). The Se spectra is fitted with three peaks (marked with A (53.53 and 54.39 eV) in blue color, B (54.39 and 55.25 eV) in red color and C (55.33 and 56.19 eV)) in pink color, which demonstrates three electronic environments for Se in the structure.

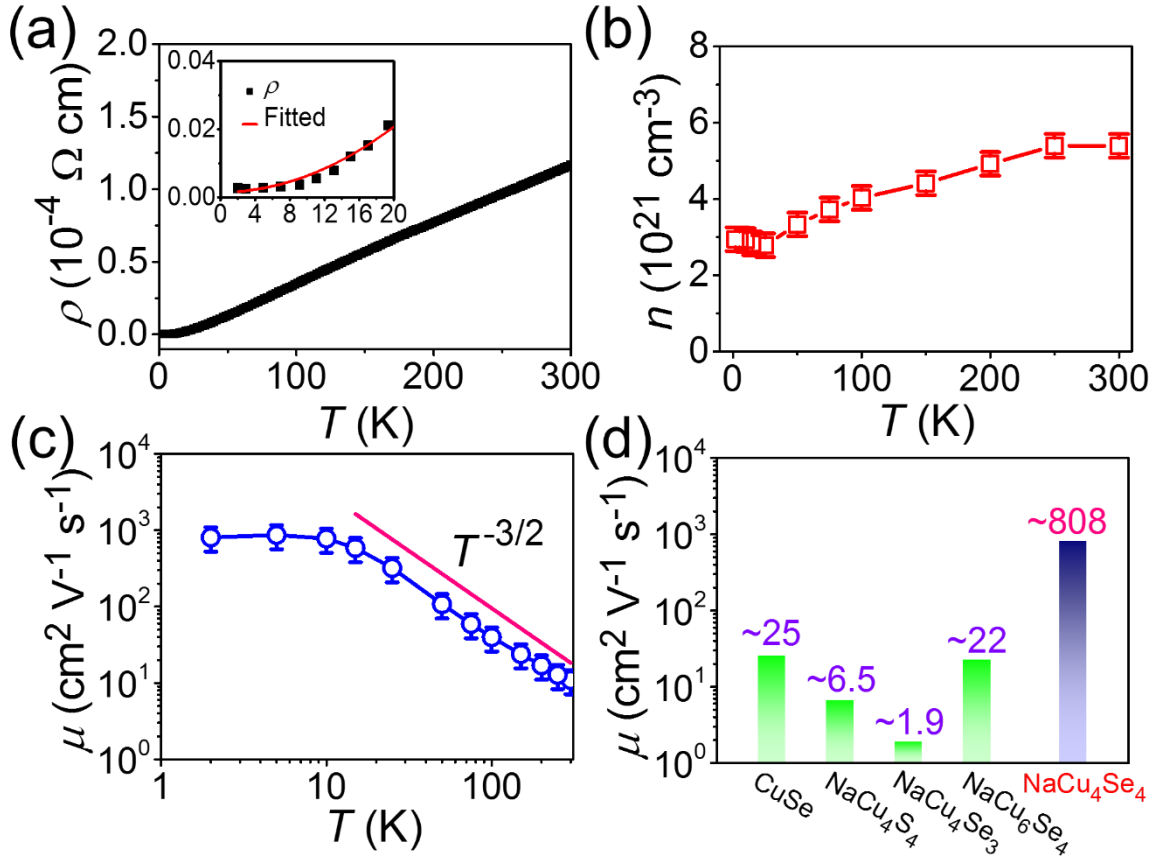


**Figure 4.** (a) Temperature dependence of the resistivity ( $\rho$ ) for NaCu<sub>4</sub>Se<sub>4</sub> from 300 K to 2 K. The data at low temperature (2 – 20 K) is well-fitted with the formula,  $0.0015 + 4.8 \times 10^{-5} T^2$  (inset). (b) Carrier density ( $n$ ) and (c) carrier mobility ( $\mu$ ) as a function of temperature. (d) Comparison of  $\mu$  values at 2 K for CuSe,<sup>59</sup> NaCu<sub>4</sub>S<sub>4</sub>,<sup>13</sup> NaCu<sub>4</sub>Se<sub>3</sub>,<sup>12</sup> NaCu<sub>6</sub>Se<sub>4</sub>,<sup>15</sup> and NaCu<sub>4</sub>Se<sub>4</sub>.

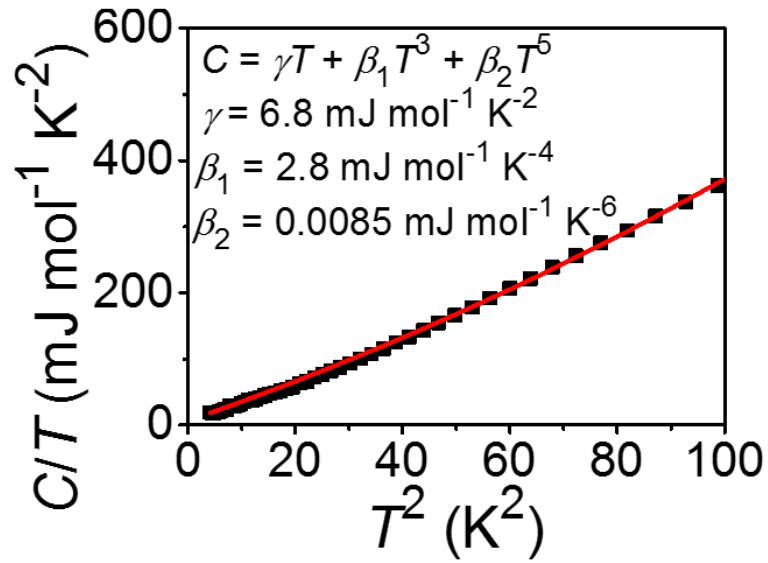


**Figure 5.** Specific heat for  $\text{NaCu}_4\text{Se}_4$  divided by temperature ( $C/T$ ) as a function of  $T^2$ . It is well fitted by the formula  $C(T) = \gamma T + \beta_1 T^3 + \beta_2 T^5$  where  $\gamma T$  and  $\beta_1 T^3 + \beta_2 T^5$  denote the electron and phonon contributions, respectively. The corresponding fitted coefficients are  $\gamma = 6.8 \text{ mJ mol}^{-1} \text{ K}^{-2}$ ,  $\beta_1 = 2.8 \text{ mJ mol}^{-1} \text{ K}^{-4}$ , and  $\beta_2 = 0.0085 \text{ mJ mol}^{-1} \text{ K}^{-6}$ , respectively.

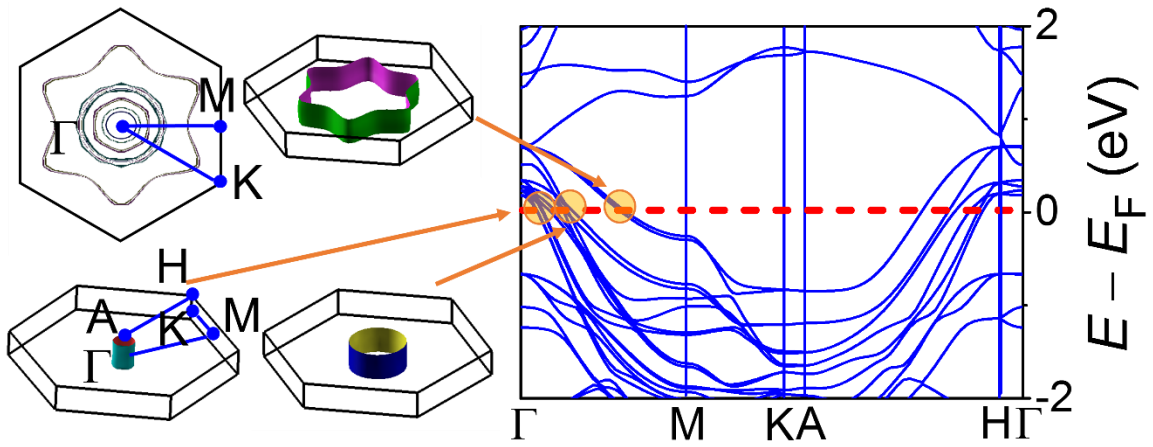


**Figure 6.** Calculated electronic band structure near the Fermi level for  $\text{NaCu}_4\text{Se}_4$  (on the right), with the Fermi surfaces (at the points in the high-symmetry path) shown on the left.

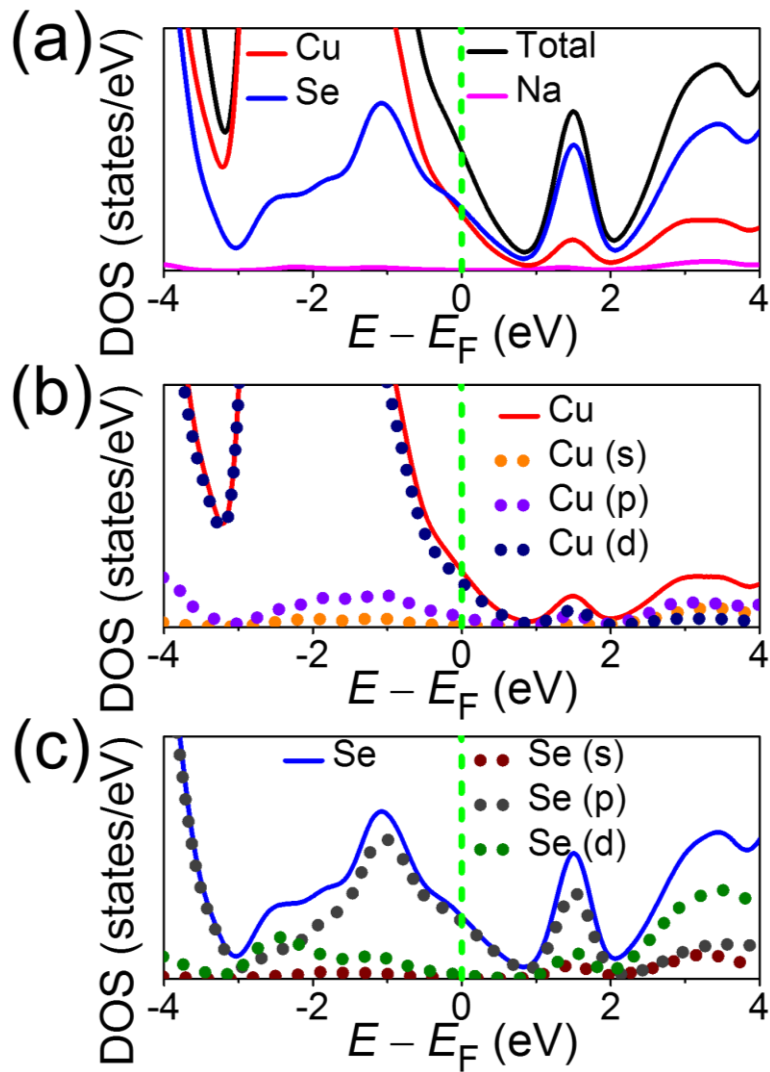


**Figure 7.** Calculated density of states (DOS) of  $\text{NaCu}_4\text{Se}_4$ , together with the projected DOS on (a) the sodium, copper and selenium atoms, (b) the  $s$ ,  $p$  and  $d$  orbitals of the copper and (c) the selenium atoms.

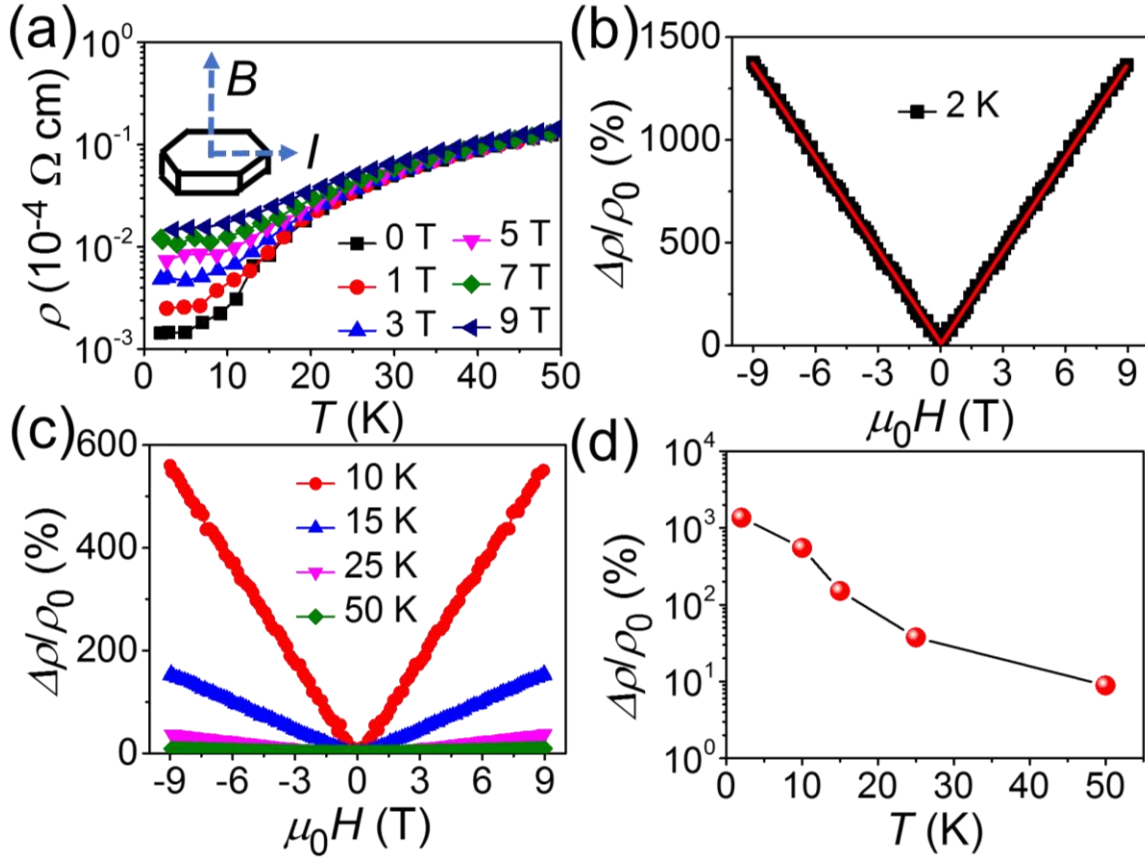


**Figure 8.** (a) Temperature dependence of resistivity ( $\rho$ ) for NaCu<sub>4</sub>Se<sub>4</sub> from 300 K to 2 K at different magnetic fields (0 – 9 T). (b) Magnetic field dependence of the magnetoresistance ( $\Delta\rho/\rho_0$ ) at 2 K, defined as  $[\rho(H) - \rho(0)]/\rho(0) \times 100\%$ , displays a linear behavior. (c)  $\Delta\rho/\rho_0$  at different temperatures (10 – 50 K). (d) Change of  $\Delta\rho/\rho_0$  at 9 T with different temperatures.



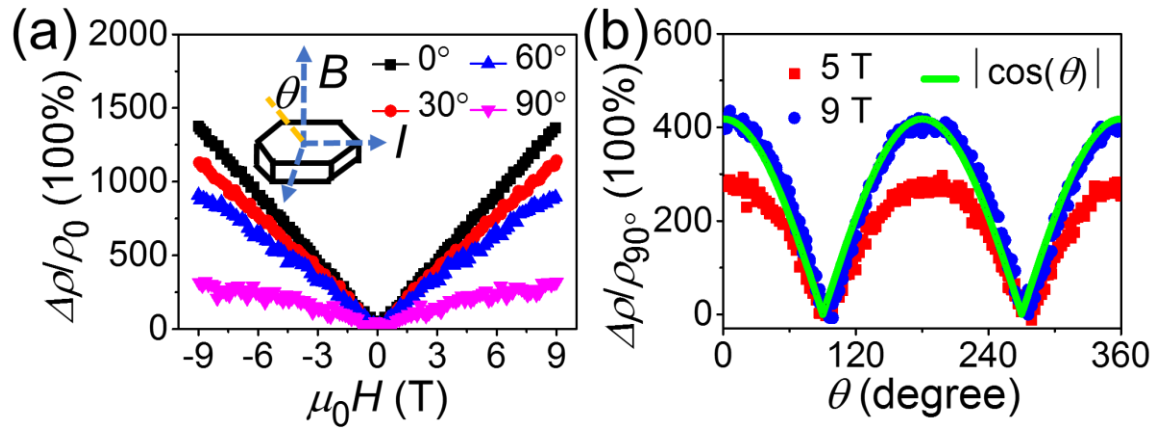


**Figure 9.** (a) Field dependence of magnetoresistance ( $\Delta\rho/\rho_0$ ) at 2 K, defined as  $[\rho(H) - \rho(0)]/\rho(0) \times 100\%$ , at an angle  $\theta$  of  $0^\circ$ ,  $30^\circ$ ,  $60^\circ$ , and  $90^\circ$ .  $\theta$  is the angle between the field and the crystallographic  $c$  axis. (b) Tilt angle dependence of magnetoresistance ( $\Delta\rho/\rho_{90^\circ}$ ), defined as  $[\rho(H) - \rho_{90^\circ}]/\rho_{90^\circ} \times 100\%$ , from  $0^\circ$  to  $360^\circ$  at a magnetic field of 9 and 5 T at 2 K.  $\Delta\rho/\rho_{90^\circ}$  is well fitted by the  $|\cos(\theta)|$  function.

For Table of Contents Only

